ADVANCED ELECTRONIC MATERIALS
www.advelectronicmat.de

# Real-Time Correlation Detection via Online Learning of a Spiking Neural Network with a Conductive-Bridge Neuron

*Dong-Won Kim, Dae-Seong Woo, Hea-Jee Kim, Soo-Min Jin, Sung-Mok Jung, Dong-Eon Kim, Jae-Joon Kim, Tae-Hun Shim, and Jea-Gun Park**

**The neuronal density of complementary metal-oxide-semiconductor field-effect transistor-based neurons is limited because of the use of capacitors. Therefore, a novel neuron is fabricated using a conductive-bridge-neuron device, current-mirror-type sense amplifier, latch, micro-controller-unit, and digital-analog-converters. This neuron exhibits a typical integrate-and-fire function; in particular, the generation frequency of the fire spikes at the neuron exponentially increases with the input-voltage-spike amplitude. Using the proposed designed neuron in combination with an input spike generation and spike-timing-dependent-plasticity algorithm, a real-time correlation detection based on online learning is realized. With the increase in the number of learning iterations, the weight of synapses for 100 correlated input neurons gradually increase, whereas that for 900 uncorrelated input neurons steadily reduce. In addition, after 700 learning iterations, the output neuron is almost synchronized with the 100 correlated input neurons, thereby achieving correlation detection for cognitive functions in neuromorphic architectures and demonstrating the possibility of development of a neuromorphic chip based on the conductive-bridge neurons and synapses.**

## 1. Introduction

Bioinspired neuromorphic computing architectures have emerged as promising alternatives for conventional von Neumann architectures to overcome the von Neumann bottleneck in artificial intelligence applications.[1–8] Neuromorphic architectures, especially spiking neural networks (SNNs), consume considerably less power (≈20 mW), than conventional von Neumann computing architectures (≈100 W).[9] As the main building block of SNNs, spiking neurons, especially complementary-metal-oxide-semiconductor field-effect transistor (C-MOSFET)-based neurons, have been intensively researched. However, the density of such neurons is limited because of the extremely large area of the capacitor (>500 $\mu m^2$ per capacitor) required to emulate the integrate function and achieve sufficient capacitance (i.e., several pF per capacitor).[10–18] To overcome this problem, the use of capacitor-less spiking neurons has been recommended. Recently, several researchers reported spiking neurons that can exhibit the integrate functionality, based on frameworks such as the phase-change memory,[19,20] resistive-random-access memory,[21–25] conductive-bridge-random-access memory,[26,27] and partially depleted silicon-on-insulator.[28] A spiking neuron principally needs a spike neuron device to emulate the integrate function and a sensing amplifier circuit to generate the fire function in a scheme known as integrate-and-fire. However, the existing studies only empirically presented spiking neuron devices to emulate the integrate function. Certain researchers designed a neuron in software by using a sense amplifier circuit, a controller for operating the neuron, a SNN containing neurons, and synapses, and a pattern recognition test was conducted using software simulations. However, only the realization of a spiking neuron was demonstrated as all the SNN operations based on spiking neuron devices emulating the integrate function were conducted via simulations.

This study represents the first attempt at developing a conductive-bridge neuron emulating an integrate-and-fire function as an alternative to conventional C-MOSFET-based spiking neurons. The neuron was composed of a conductive-bridge-neuron device, sensing amplifier, and latch circuit. The conductive-bridge-neuron device was fabricated in a simple manner by adopting a vertical device structure including a CuTe top electrode, $TiO_2$ resistive layer, and TiN bottom electrode. The Cu atoms diffused from the CuTe top electrode could easily form Cu filaments in the $TiO_2$ resistive layer. This phenomenon is of significance because Cu filaments in the $TiO_2$ resistive

D.-W. Kim, D.-S. Woo, H.-J. Kim, S.-M. Jin, S.-M. Jung, J.-G. Park
Department of Nano-scale Semiconductor Engineering
Hanyang University
Seoul 04763, Republic of Korea
E-mail: parkjgl@hanyang.ac.kr
D.-E. Kim, J.-G. Park
Department of Electronic Engineering
Hanyang University
Seoul 04763, Republic of Korea
J.-J. Kim
Department of Electrical and Computer Engineering
Seoul National University
Seoul 08826, Republic of Korea
T.-H. Shim, J.-G. Park
Advanced Semiconductor Materials and Devices Development Center
Hanyang University
Seoul 04763, Republic of Korea

The ORCID identification number(s) for the author(s) of this article can be found under https://doi.org/10.1002/aelm.202101356.



**DOI: 10.1002/aelm.202101356**

layer principally influence the integrate function of a neuron device (i.e., the integrated voltage increase behavior as the number of input-current spikes increases). In addition, a SNN was designed with a hardware conductive-bridge neuron as an output neuron, a software synaptic weight update strategy based on the simplified spiking-timing-dependent-plasticity (STDP) algorithm, and a software signal control scheme (i.e., neuron circuit control and output signal sensing from the neuron) based on a micro controller. The hardware neuron was used to examine the dependence of the number of fire spikes on the input-voltage-spike amplitude. Using the SNN with the integrate-and-fire function and simplified STDP algorithm, the possibility of real-time correlation detection for cognitive functions in pattern or voice recognition was tested.

## 2. Results and Discussion

### 2.1. Conductive-Bridge-Neuron Device

To realize SNN neuromorphic chips with a high neuronal density unlike C-MOSFET-based SNNs, a neuron should be designed with one neuron device and the least number of n- and p-MOFSETs without capacitors. To this end, a conductive-bridge-neuron device is a promising framework. The device was fabricated to have a vertical structure including a 100-nm-thick CuTe top electrode, 15-nm-thick $TiO_2$ resistive layer, and 100-nm-thick TiN bottom electrode, as shown in **Figure 1**a. The area of the conductive-bridge-neuron device was $5 \times 5$ μm$^2$. The Cu ion concentration in the context of the

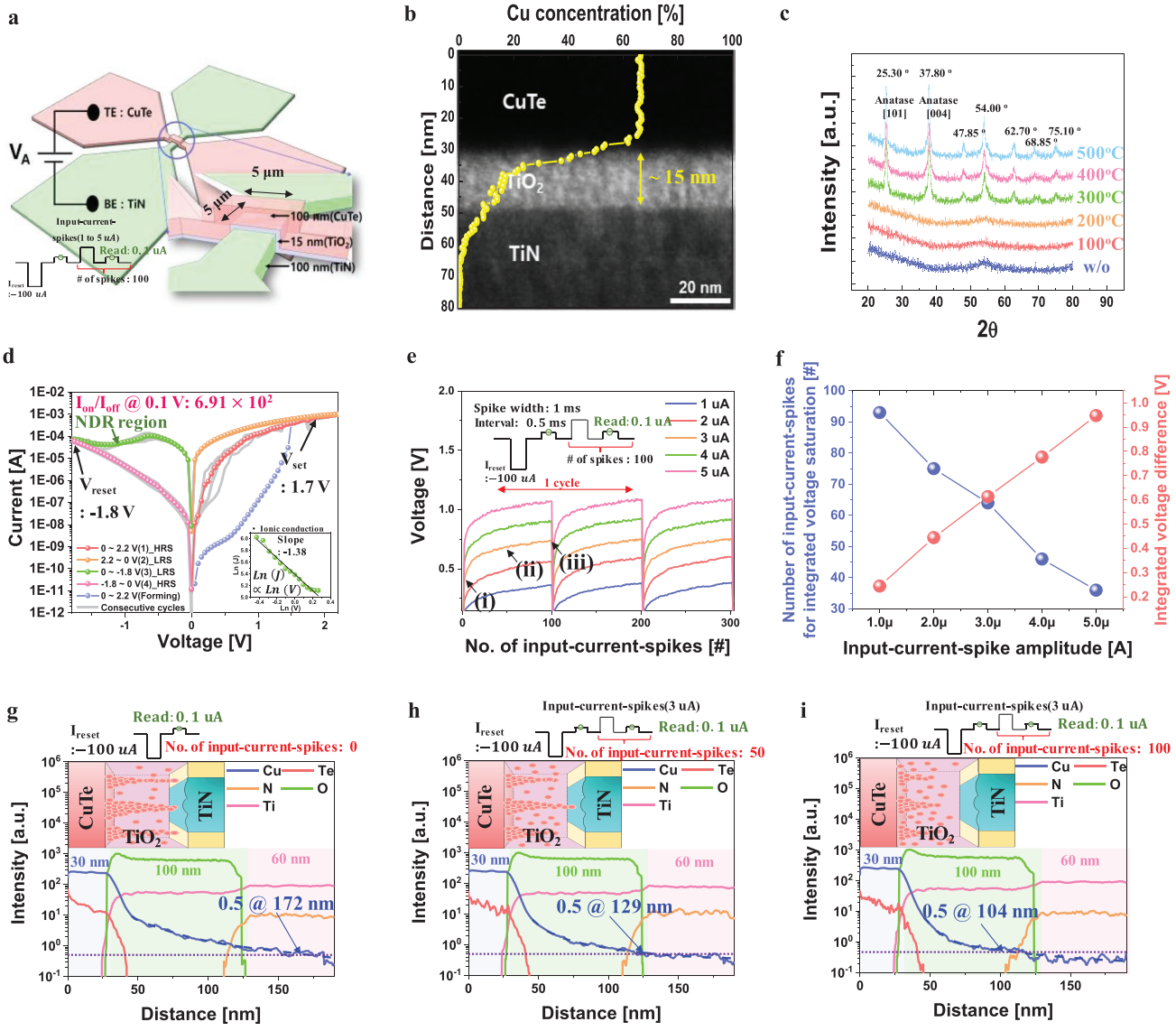


**Figure 1.** Conductive-bridge-neuron device. a) Device structure. b) Depth profile of Cu ion concentration, analyzed through EDS line-scanning and x-TEM image. c) Crystallinity of $TiO_2$ resistive layer at without and different additional annealing temperatures, analyzed by X-ray diffraction. d) *I–V* curve. e) Integrate function depending on the input-current-spike amplitude. f) Number of input-current spikes for integrated voltage saturation (blue) and difference (red) depending on the input-current-spike amplitude. g) Depth profile of Cu ion concentration after reset. h) Depth profile of Cu ion concentration after inputting 50 current spikes. i) Depth profile of Cu ion concentration after inputting 100 current spikes.

complementary-error-function decreased from the top electrode (≈66%) to the bottom electrode (≈3%). Therefore, inverse-conical-shaped Cu filaments would be produced in the $TiO_2$ resistive layer as the Cu ions diffused from the CuTe top electrode during sputtering of the top electrode, as shown in Figure 1b.[29–31] The surface roughness of the TiN bottom electrode was investigated by using atomic force microscope, as shown in Figure S1, Supporting Information. Several locations like a hillock were found in the area (1 $\mu m^2$) of the TiN bottom electrode, where a higher electric field would be applied at hillocks rather than valleys. Thus, multiple Cu filaments would be produced in the $TiO_2$ resistive switching layer on the TiN bottom electrode. In addition, it was reported that a CBRAM included multiple metallic filaments in the resistive switching layer.[30,31]

In addition, the $TiO_2$ resistive layer having an amorphous structure, not subjected to additional annealing, was selected because a high resistance state (HRS) of the $TiO_2$ resistive layer is essential for achieving a significantly HRS, as shown in Figure 1c. Note that an additional annealing above 200 °C transformed the crystallinity of the $TiO_2$ resistive layer from amorphous to anatase structure and the resistance of the $TiO_2$ resistive layer having an amorphous structure would be generally higher than that having crystalline structure.[32] To confirm the presence of Cu filaments in the $TiO_2$ resistive layer, the voltage was scanned from 0 to 2.2 V; the current rapidly increased with the applied bias between the top and bottom electrodes, resulting in the formation of Cu filaments. The current-versus-voltage (*I*–*V*) curve for the conductive-bridge-neuron device exhibited the HRS, low resistance state (LRS), LRS, and HRS, when the applied bias between the top and bottom electrodes was scanned from 0 to 2.2 V, –1.8 V, and 0 V, similar to that of a CBRAM, with a $V_{set}$ of 1.7 V and $V_{reset}$ of –1.8 V, as shown in Figure 1d.[29–31] After forming process, the conductive-bridge-neuron device showed the on/off ratio of $6.91 \times 10^2$ at 0.1 V. The cumulative average voltage and standard deviation for the formation process were 1.66 and 0.21 V, respectively, whereas those for the set process were 1.64 and 0.18 V, respectively, indicating the reliable electrical characteristics of the neuron device, as shown in Figure S2, Supporting Information. In particular, to operate a conductive-bridge-neuron device performing integrate function, the negative differential resistance (NDR) region was selected, which means the integrate function of conductive-bridge-neuron device would be performed by the rupturing process of the conductive Cu filaments in the $TiO_2$ resistive layer, as shown in the green line of Figure 1d. The current conduction of the NDR region was followed by ionic conduction mechanism, as shown in inset of Figure 1d. To implement the integrate function, $I_{reset}$ of –100 μA was initially applied to form Cu filaments in the $TiO_2$ resistive layer, thereby attaining an LRS, as indicated by the orange line in Figure 1d. Note that set process happened at the positive applied bias since the conductive-bridge-neuron device behaves as a CBRAM; otherwise, set process would be found at the negative applied bias if the conductive-bridge-neuron device behaves as an OxRAM. Thus, the conductive-bridge-neuron device follows evidently the CBRAM mechanism. In addition, the LRS current in the conductive-bridge-neuron device decreased clearly with increasing the device operation temperature, indicating that the resistive switching layer includes metallic (Cu) filaments, as shown in Figure S3, Supporting Information.[33,34] Remind that the LRS current for OxRAM having oxygen vacancy filaments in the resistive switching layer increases with the operation temperature.[35–37] Moreover, the dependency of the LRS current on the device operation temperature for the conductive-bridge-neuron device proved that the conductive-bridge-neuron device was a CBRAM having Cu filaments, since Te behaves as a semiconductor rather than a metallic characteristic where the LRS current decreases as the device operating temperature increases.[38] The device resistance increased with the input-current spikes, thereby attaining the HRS, as indicated by the green line in Figure 1d. This result indicates that the Cu filaments formed and ruptured when the input-current spikes increased, emulating an integrate function. The reason why CuTe as a metal filament source rather than Cu or Ag in the conductive-bridge-neuron device was associated with the achievement of a self-compliance current limit at set process or not, as shown in Figure S4, Supporting Information. The conductive-bridge-neuron device having CuTe top electrode could perform a self-compliance current limit at set process, while those having Cu or Ag top electrode were essentially necessary for applying a compliance current limit at set process. In particular, the composition ratio between Cu and Te of 6:4 could the achievement of a self-compliance current limit at set process.[39] Our proposed conductive-bridge-neuron device was used the CuTe top electrode having 6:4 composition ratio. The importance of a self-compliance current limit is that the presence of a self-compliance current limit in the conductive-bridge-neuron device can avoid a breakdown of the conductive-bridge-neuron device. The additional circuit to avoid a breakdown of conductive-bridge-neuron device should be necessary if the conductive-bridge-neuron device should use a compliance current at set process. A negative current spike having a spike amplitude of –100 μA was applied, and hundreds positive input-current spikes (i.e., pulses) with a 1 ms spike width were sequentially applied on the TiN bottom electrode. The input-current-spike amplitude was varied from 1 to 5 μA, as shown in Figure 1e, which is the schematic of the input-current spikes in one cycle. The voltages of the neuron device induced between the top and bottom electrodes were measured between the read operation. As the number of input-current spikes increased, the integrated voltage of the conductive-bridge-neuron device gradually increased and saturated, emulating a typical integrate function, as shown in Figure 1e. As the amplitude of input-current spikes was further increased, the number of input-current-spikes for integrated voltage saturation linearly decreased, as shown in Figure 1f. Therefore, the integrated voltage difference linearly increased with the amplitude of input-current spikes. In addition, since the conductive-bridge-neuron device showed gradually an integrate behavior as the number of input-current-spikes increases; the effective multilevel states were evidently divided into 32 levels, as shown in Figure S5, Supporting Information.

To prove the mechanism by which the conductive-bridge-neuron device emulated integrate function, intentional conductive-bridge-neuron devices having the area of $60 \times 60$ $\mu m^2$ were fabricated, and the depth profiles of Cu ion concentration between top and bottom electrode were characterized as a function of after reset (LRS) in (i) of Figure 1e, after inputting 50 current spikes in (ii) of Figure 1e, and after inputting 100 current

spikes in (iii) of Figure 1e, as shown in Figure 1g–i. Note that these devices were fabricated to have a vertical structure including a 30-nm-thick CuTe top electrode, 100-nm-thick $TiO_2$ resistive layer, and 60-nm-thick TiN bottom electrode. In addition, the depth profile of Cu ion concentration was measured by time-of-flight secondary ion mass spectrometry (ToF-SIMS). For the conductive-bridge-neuron device after reset (LRS), the relative Cu ion concentration from top to bottom electrode decreased from $\approx 2.61 \times 10^2$ to 0.5 intensity (arbitrary unit: a.u.) at 42 nm under the TiN bottom electrode (i.e., 130 nm in depth from the surface of the CuTe top electrode) with the context of complementary error function, as shown in Figure 1g.

This result indicates that inverse-conical-shape Cu filaments were formed in the $TiO_2$ resistive layer, as shown in the inset of Figure 1g. Otherwise, for the conductive-bridge-neuron device after inputting 50 current spikes, the relative Cu ion concentration from top to 1 nm above bottom electrode (i.e., 130 nm in depth from the surface of the CuTe top electrode) decreased from $\approx 2.68 \times 10^2$ to 0.5 intensity (a.u.), as shown in Figure 1h. The positive-charged Cu ions in the $TiO_2$ resistive layer drifted from the bottom to top electrode as the positive 50 current pulses were supplied from bottom electrode. Thus, the Cu ion concentration near bottom electrode after inputting 50 current spikes was significantly reduced compared to that after reset, thereby enhancing the resistance of the conductive-bridge-neuron device. This result means that some of Cu filaments in the $TiO_2$ resistive layer would be ruptured after inputting 50 current spikes, as shown in the inset of Figure 1h. Moreover, for the conductive-bridge-neuron device after inputting 100 current spikes, the relative Cu ion concentration from top to 26 nm above bottom electrode (i.e., 130 nm in depth from the surface of the CuTe top electrode) decreased from $\approx 2.7 \times 10^2$ to 0.5 intensity (a.u.), as shown in Figure 1i. The Cu ion concentration near bottom electrode after inputting 100 current spikes was further remarkably decreased compared to that after inputting 50 current spikes. This result implies that most of Cu filaments in the $TiO_2$ resistive layer would be ruptured, as shown in the inset of Figure 1i. Comparing Figure 1g–i, as the number of input-current-spikes increased from 0 to 50 and 100, the depth of the Cu ion intensity being arrived at 0.5 a.u. moved from 172 to 129 and 104 nm, as shown in Figure S6, Supporting Information. This result indicated that the mechanism by which the conductive-bridge-neuron device emulated integrate function was associated with the increase of the rupturing degree of the Cu filaments in the $TiO_2$ resistive layer as a number of input-current spikes increased.

### 2.2. Fabrication of Conductive-Bridge Neuron

In a biological neural network, neurons communicate with other neurons through synapses using spike signal, as shown in Figure S7a, Supporting Information. The magnitude of the transmitted spike signal from the pre-neuron to the post-neuron is determined by the weight of the synapse between these neurons. When a post-neuron receives pre-synaptic spikes (input spikes) from pre-neurons, the membrane potential ($V_{mem}$) of the post-neuron increases with the number of input spikes, corresponding to the integrate function. When the membrane potential exceeds a certain threshold ($V_{th}$), the post-neuron generates a post-synaptic spike, that is, fire function, as shown in Figure S7b, Supporting Information. Subsequently, the post-synaptic spike propagates to the adjacent neurons connected to the post-neuron to update the synaptic weight at the synapses between the post-neuron and adjacent neurons. This neuronal dynamic known as integrate-and-fire is widely identified as a neuron model describing the neuron behavior of biological neural network.[40,41] To emulate the integrate-and-fire at an artificial spiking neuron, similar to a biological spiking neuron, the post-neuron was connected with a pre-neuron through synapses, and a controller including a clock, read, integrate, $V_{integrate}$, and output spikes was established, as shown in **Figure 2**a. The artificial neuron emulating the integrate-and-fire function was realized using one conductive-bridge-neuron device, seven n-MOSFETs, three p-MOSFETs, and one reference resistor ($R_{ref}$) to minimize the core area of the neuron ($\approx 8\ \mu m^2$, through an 28 nm C-MOSFET process), as shown in Figure S8, Supporting Information.[42] To overcome the limitation of lab-scale neuron fabrication based on discrete C-MOSFETs and resistors—specifically, the difficulty in matching the transistor specifications for the latch-type sense amplifier, as indicated in Figure S8, Supporting Information—a current-mirror-type sense amplifier and latch were designed to operate the lab-scale neuron by using a conductive-bridge-neuron device, as shown in Figure 2b. Thus, a lab-scale conductive-bridge-neuron composed of a conductive-bridge-neuron device placed on a probe station, a current-mirror-type sense amplifier, and a latch was generated. The amplifier was produced using discrete C-MOSFETs and resistors implemented on a breadboard, as shown in Figure S9, Supporting Information.

In addition, DACs, power supply, and MCU were used to produce the read, integrate, $V_{integrate}$, and latch-reset spike, as shown in Figure S9, Supporting Information; the timing diagram is shown in Figure 2b. Read (1.7 V), integrate (5 V), $V_{integrate}$ (1.7–1.8 V), and latch-reset (5 V) spikes were sequentially supplied through the MCU; the integrate and $V_{integrate}$ spikes were simultaneously provided through the MCU and DAC, as shown in the timing diagram in Figure 2a. $V_{DD}$–$V_{reset}$ (2.8 V) was applied on the bottom electrode of the conductive-bridge-neuron device, and a high voltage (4 V) at the $V_1$ node was initially sustained by the latch, as shown in Figure 2b. When the integrate and $V_{integrate}$ spikes were applied to the gate electrodes of $V_{integrate}$ and integrate n-MOSFETs, the applied voltage on the conductive-bridge-neuron device increased. When the integrate and $V_{integrate}$ spikes were continuously applied, the applied voltage on the conductive-bridge-neuron device continuously and gradually increased, emulating an integrate function. The read spike was synchronized with the integrate, $V_{integrate}$, and latch-reset spikes to compare the induced voltage between the $V_2$ node and $V_{ref}$ (i.e., reference voltage), and the fire spike were sequentially generated if the induced voltage at the $V_2$ node was less than 2.01 V, thereby achieving the fire function.

Using the developed neuron, as shown in Figure 2b and Figure S9, Supporting Information, the dependence of the integrate-and-fire function on the number of input-voltage spikes (i.e., $V_{integrate}$ in Figure 2b) for the conductive-bridge neuron was evaluated as a function of the input-voltage-spike amplitude, as shown in **Figure 3** and Video S1, Supporting Information.

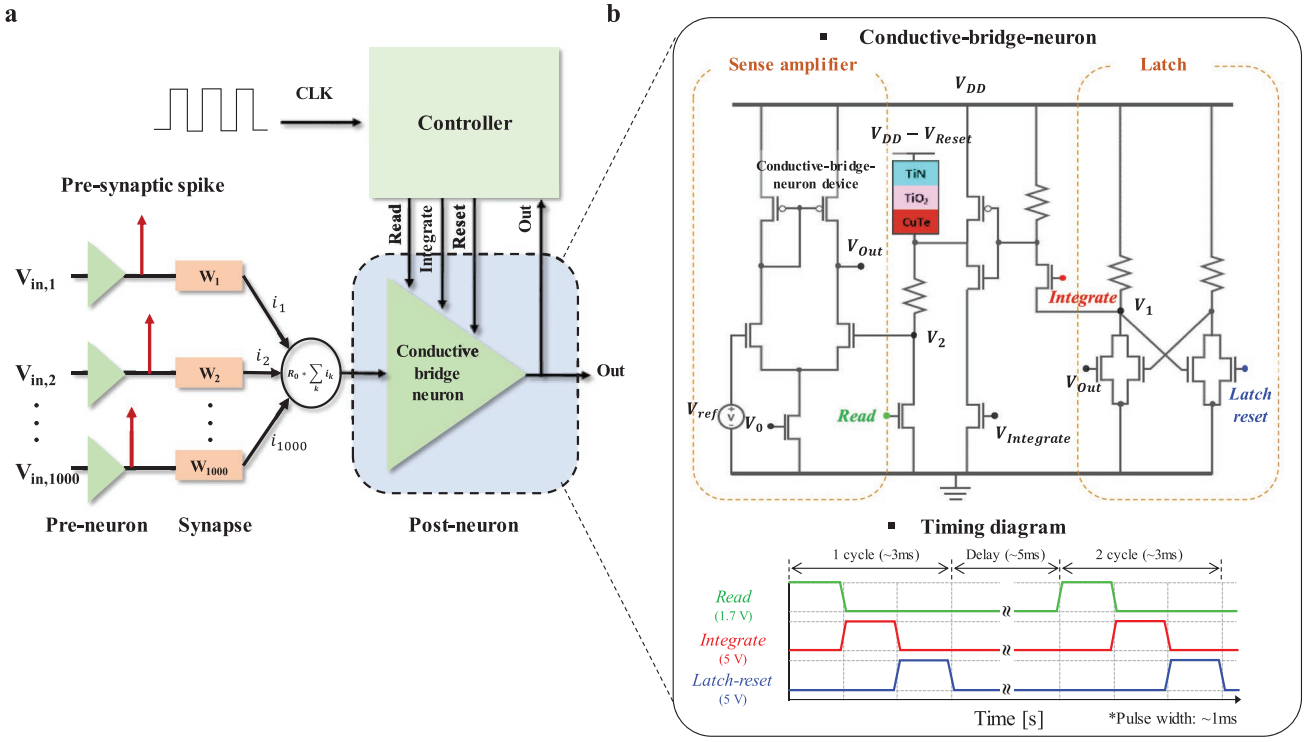


**Figure 2.** Conductive-bridge neuron. a) Schematic of spiking neural network (SNN) designed with a conductive-bridge neuron (i.e., output neuron), controller, synapses, and input neurons. b) Conductive-bridge-neuron circuit design emulating the integrate-and-fire function by using a conductive-bridge-neuron device, current-mirror-type sense amplifier, and latch. One cycle in the timing diagram involves read, integrate, $V_{integrate}$, and latch-reset signals.

The input-current spikes were sequentially applied on the bottom electrode of the conductive-bridge-neuron device because the input-voltage spikes at the $V_{integrate}$ node were sequentially applied, as shown in Figure 2b. At the input-voltage-spike amplitude of 1.70 V, an integrate-and-fire mechanism occurred after 134 input-voltage spikes, thereby generating a fire spike (i.e., output spike) at the $V_{out}$ node shown in Figure 2b, as shown in Figure 3a. When the input-voltage spikes were continuously and sequentially supplied after resetting the latch circuit shown in Figure 2b, an additional integrate-and-fire occurred after ≈276 input-voltage spikes. These results indicated that the number of input-voltage spikes (≈134) that generated the first fire spike was different from that (≈410) of the spikes that generated the second fire spike. This phenomenon can be attributed to the variation in the integrated voltage with the increase in the number of input-current spikes, as shown in Figure 1e. The dependence of the generation of the fire spikes was examined as the input-voltage-spike amplitude increased from 1.70 to 1.80 V in increments of 0.01 V, as shown in Figure 3a–k. The fire spikes were generated earlier at a higher input-voltage-spike amplitude, indicating that a higher input-voltage-spike amplitude led to a higher generation frequency of the fire spikes. Although the interval of the occurrence of fire spikes was not identical, the optimization of a SNN was not expected to be a critical issue owing to the similarity with the human-brain neuron behavior, as shown in Figure 3a–k. In particular, the generating frequency increased almost exponentially with the input-voltage-spike amplitude, as shown in Figure 3l. The increase in the generation frequency of the fire spikes with the input-voltage-spike amplitude could be understood by considering conductive Cu filaments in the $TiO_2$ resistive layer against the electric-field applied to the resistive layer including $Cu^{2+}$ ions.[29–31] Because the migration probability of the $Cu^{2+}$ ions in the resistive layer (i.e., 15-nm-thick $TiO_2$) increased with the applied electric-field intensity on the conductive-bridge-neuron device, the Cu filaments became thinner in the resistive layer when the input-voltage-spike amplitude increased, as shown in Supporting Information Note.

### 2.3. Real-time Correlation Detection with Online Learning for SNN Using Conductive-Bridge Neuron

Human brains receive a continuous sensory stream from the retina, lateral geniculate cortex, and striate cortex, among other entities, and can efficiently and simultaneously manage these multisensory bio-signals. The mechanisms by which the brain processes multisensory signals are closely related to the ability of neurons capturing the correlations among the multisensory signals. In addition, correlation detection (also known as coincidence detection) plays a critical role in the learning and memory activities in the human brain.[43–45] The importance of the integrate-and-fire function in the realization of the real-time correlation detection can be understood by the recognition process of the human brain. When the human brain receives continuous multisensory bio-signals in real-time, each neuron in the human brain combines (i.e., integrate function) the multisensory bio-signals and generates output bio-signals (i.e., fire function) being transferred

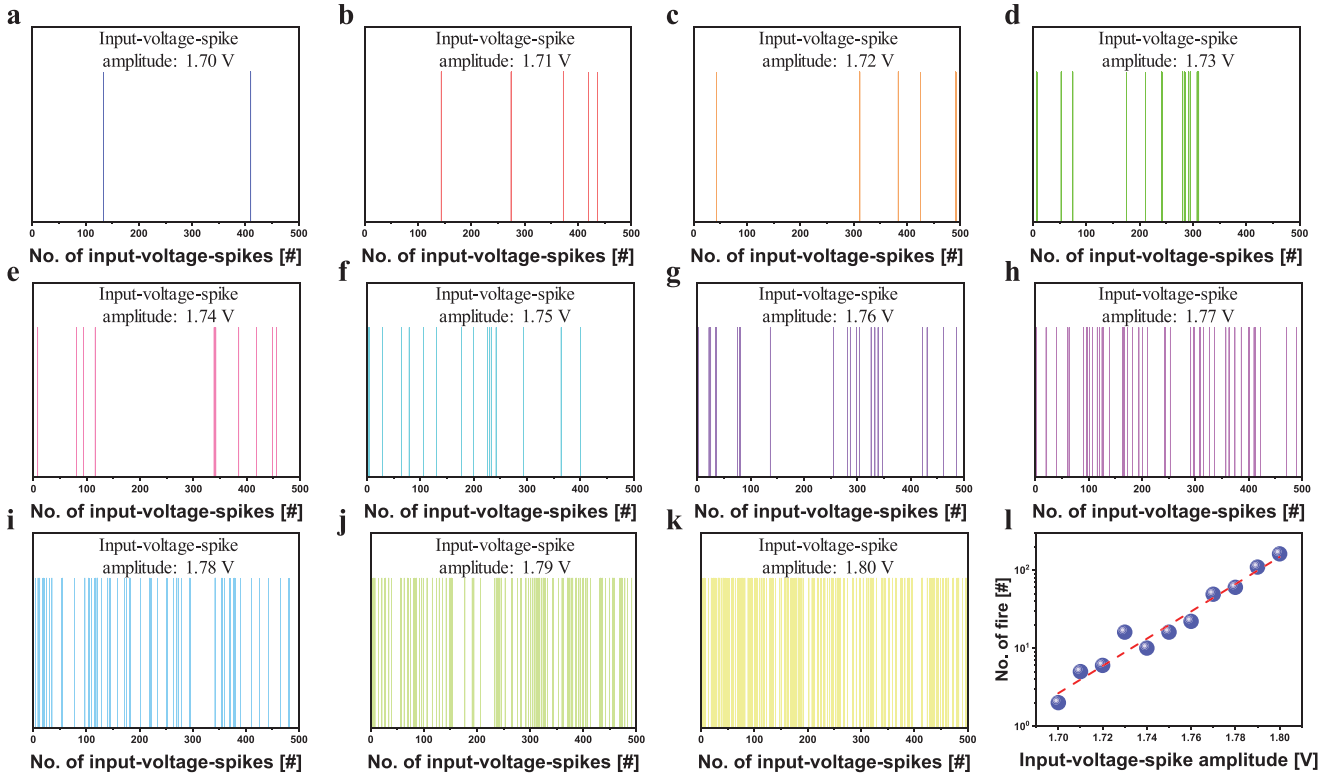


**Figure 3.** Integrate-and-fire function of conductive-bridge neuron. a–k) Frequency of fire generation depending on the input-voltage-spike amplitude variation from 1.70 to 1.80 V in increments of 0.01. l) Variation in the number of fires with the input-voltage-spike amplitude.

toward other neurons via synapses. The learning processes in the human brain to update the synapses connected with the correlated pre-neurons were conducted by using a specific STDP learning rule. As a result, the fire activity of pre-neuron was synchronized with that of post-neuron, indicating a specific recognition for a specific bio-signal. Hence, correlation detection must be ensured to realize cognitive functions in neuromorphic architectures. To examine the feasibility of correlation detection based on the proposed approach, a SNN was designed, as shown in **Figure 4**. The software part was composed of the input spike generation module, simplified STDP algorithm, and graphical user interface (GUI) to control

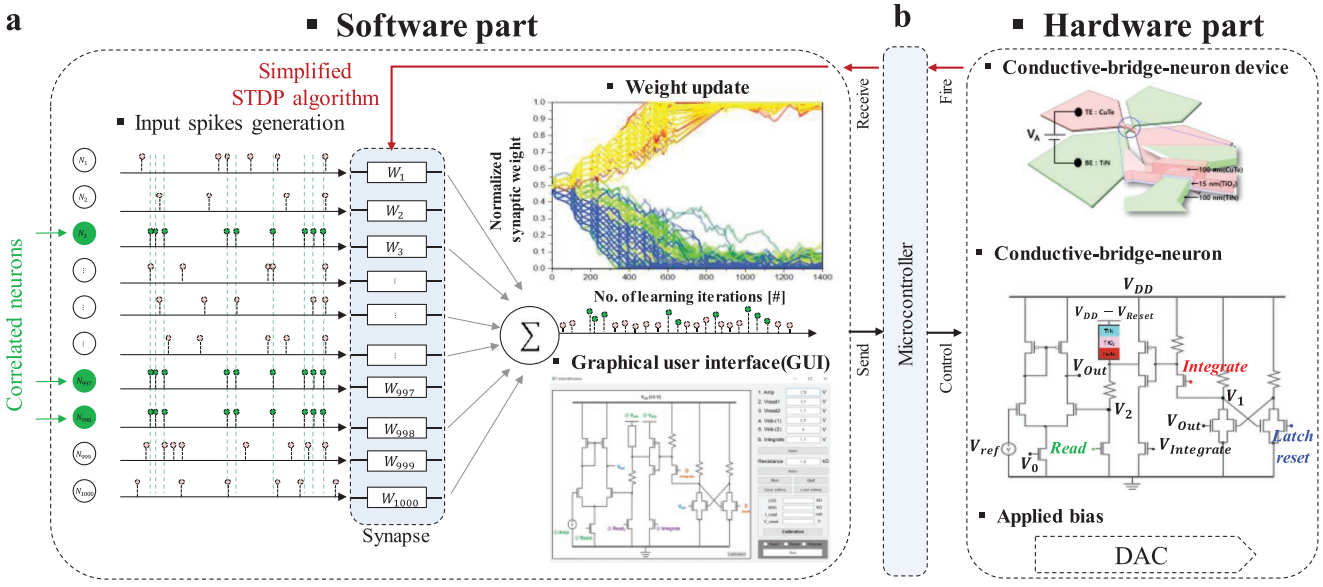


**Figure 4.** SNN with hardware and software parts. a) Software part with 1000 input neurons, input spike generation module, 1000 synapses, STDP algorithm, and GUI controlling the conductive-bridge neuron. b) Hardware part with the conductive-bridge neuron, MCU, and DACs.

the neuron, and the SNN was composed of 1000 input neurons, 1000 synapses, and one output neuron. The hardware part included the conductive-bridge neuron, DACs, and MCU, as shown in Figure 2 and Figure S9, Supporting Information. All the synapses were initialized with a weight of 0.5. In the software part, input spikes penetrating 1000 input neurons were generated, a synaptic weighted sum was performed, and the weighted sum was transferred to the DAC via the MCU. The DAC transformed the digital weighted sum into a specific analog voltage. This analog voltage ($V_{integrate}$) was input to the neuron, and the fire spike at the $V_{out}$ node was generated as soon as $V_2$ was less than 2.01 V, as shown in Figure 2b. The simplified STDP algorithm was implemented by identifying the time difference between the occurrence of a fire spike between the input neurons and output neuron, and the weights of 1000 synapses were updated. The synaptic weights for the synapses connected with the already fired input neurons were potentiated and depressed when the fire spike time difference between the input and output neurons was less and more than five cycles, respectively. One cycle involved read, integrate, and latch-reset operations, as shown in the timing diagram in Figure 2b.

Initially, 100 and 900 correlated and uncorrelated input neurons were selected, with covariance values of 0.5 and 0, respectively. To generate these correlated and uncorrelated input fire spikes, 1000 Gaussian random numbers were generated from a multivariate-normal-probability-density function, as explained in the Experimental Section.[46] A raster plot of 1000 input neurons was generated, in which the correlated neurons were not distinguished from the uncorrelated neurons, as shown in **Figure 5**a. To classify these neurons, the raster plot was rearranged. The results indicated that 100 correlated neurons were obtained, with covariance values of 0.5, and 900 uncorrelated neurons randomly produced fire spikes, as shown in Figure 5b,c. Using the randomly distributed input fire spikes for the 100 correlated and 900 uncorrelated input neurons, the SNN shown in Figure 4 was trained and a time evolution of the normalized synaptic weight was produced, as shown in Figure 5d,e. The normalized synaptic weight for the synapses connected with the 100 correlated input neurons increased gradually with the number of cycles (i.e., number of learning iterations), whereas the weight for the synapses connected with the 900 uncorrelated input neurons decreased steadily with the number of cycles.

To visualize the dependency of the raster plot on the presence or absence of the correlation at the input neurons, the number of synapse against the synaptic weight was observed as a function of the number of cycles, as shown in Figure 5f. After ten learning cycles, the average synaptic weight distribution did not change significantly, and the weights at all synapses were initially 0.5, as shown in the left part of Figure 5f. However, after 500 learning cycles, the average weight at the synapses connected with the correlated input neurons was significantly enhanced from 0.50 to 0.71, whereas that of the synapses connected with the uncorrelated input neurons significantly reduced from 0.50 to 0.22, as shown in the middle part of Figure 5f. As the number of cycles increased to 1000, the weight at all synapses connected with the correlated input neurons was ≈1, whereas the corresponding value for the synapses connected with the uncorrelated input neurons remarkably decreased from 0.50 to 0.10, as shown in the right part of Figure 5f.

The real-time evolution of the synaptic weight distribution of the synapses connected with the correlated and uncorrelated input neurons is clearly shown in Video S2, Supporting Information. The results indicate that with the increase in the number of cycles (i.e., number of learning iterations), the weights for the synapses connected with the correlated and uncorrelated input neurons remarkably increased and decreased, respectively, demonstrating the excellent training performance of the SNN. To examine the learning effect of the designed SNN, the dependence of the synchronization of the input and output fire spikes on the number of cycles was investigated for the correlated input neurons, as shown in Figure 5g. When the number of learning iterations was less than 700, the output neuron spikes were randomly generated without any synchronization of the input neuron spikes. Beyond this point, the synchronization of the fire spikes between the input and output neurons was significantly enhanced with the increase in the number of learning iterations. This result demonstrated that the designed SNN could realize real-time correlation detection and facilitate the development of a neuromorphic architecture for cognitive functions such as video analysis and voice recognition. Finally, the power consumption and operating frequency of our proposed SNN was simply reviewed. It is difficult to estimate accurately the power consumption and operating frequency of our proposed SNN since our proposed SNN was not fully integrated in hardware. Thus, assuming the worst cases, the peak power consumption and operating frequency of the proposed conductive-bridge-neuron itself was calculated by summing integrate, read, and reset operations. The peak power consumption of the conductive-bridge-neuron operating integrate, read, and reset were ≈2.9 μW at $V_{integrate}$ of 1.7 V, 1.4 μW at read current of 0.5 μA, and 96 μW in the conductive-bridge-neuron of Figure 2b, respectively, as shown in Table S2, Supporting Information. The operating frequency of the conductive-bridge-neuron was defined by a cycle of integrate, read, and reset and ≈125 Hz. The peak power consumption of the conductive-bridge-neuron (i.e., ≈100.3 μW) was similar to that of a previous report (i.e., maximum ≈ 100 μW),[13] demonstrating no accurate comparison. In addition, the operating frequency of the conductive-bridge-neuron (i.e., ≈125 Hz) was similar to that of the previous reports (i.e., ≈100 Hz).[47]

## 3. Conclusion

Typical C-MOSFET-based neurons can successfully emulate the integrate-and-fire function for SNNs; however, capacitors must be used to emulate the integrate function. Consequently, high neural-network integration cannot be achieved as an RC time constant of several milliseconds necessitates the use of a capacitor with a capacitance of several pF and a large area >500 μm$^2$. In contrast, the proposed neuron, shown in Figure S8a, Supporting Information, fabricated using a conductive-bridge-neuron device with an area of 113 × 113 nm$^2$, seven n-MOSFETs, three p-MOSFETs, and one resistor, could be implemented in a small area (≈8 μm$^2$) with a 28 nm technology node, as

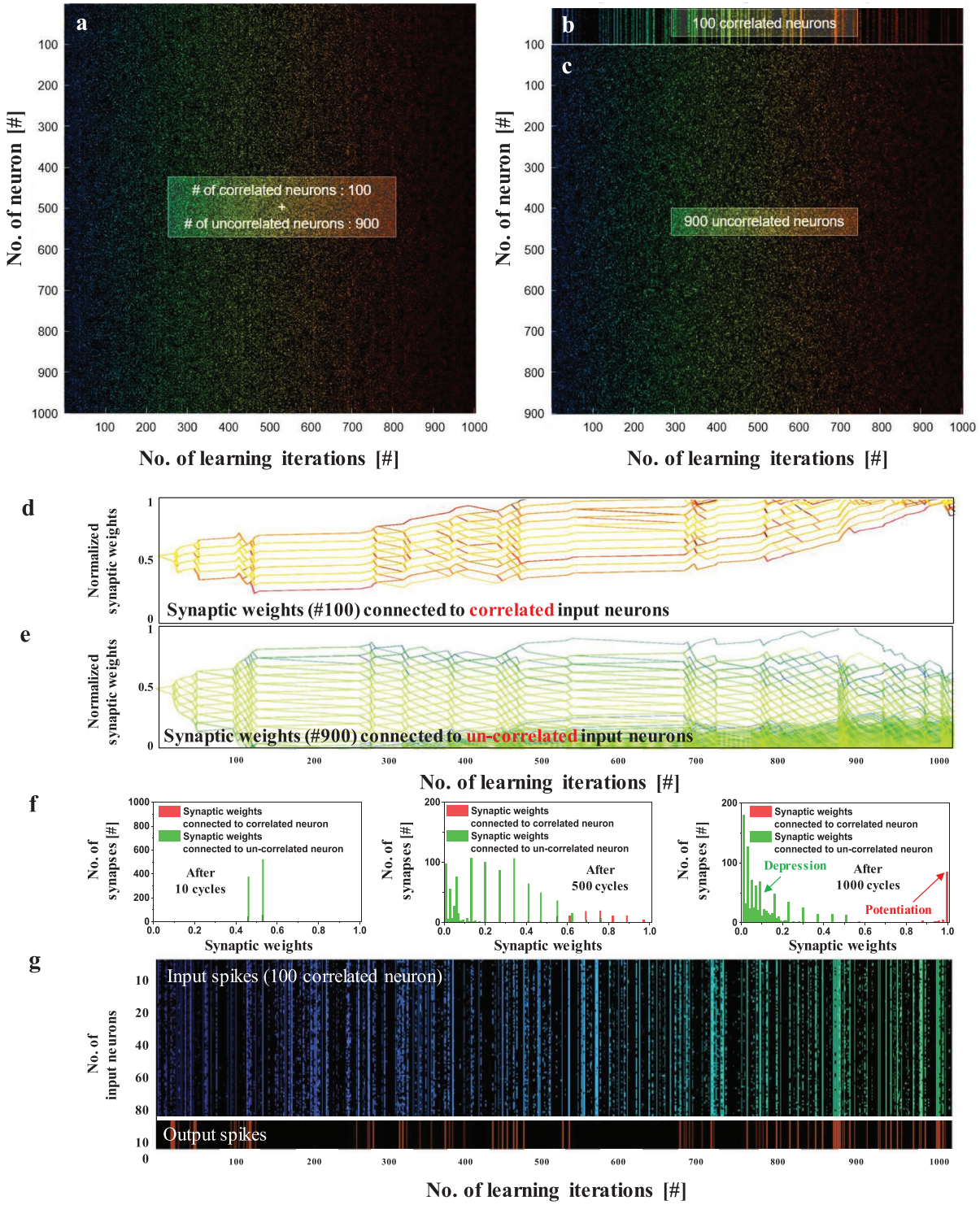


**Figure 5.** Real-time correlation detection with online learning. a) Raster plot of random input spikes with different numbers of learning iterations, with 100 correlated input spikes and 900 uncorrelated input spikes. Raster plots of the b) classified 100 correlated and c) 900 uncorrelated input spikes. d) Time evolution of weights for synapses connected with 100 correlated input neurons. e) Weights for synapses connected with 900 uncorrelated input neurons. f) Synaptic weight distribution after 10, 500, and 1000 learning iterations. g) Test results of real-time correlation detection with online learning.

summarized in Table S1, Supporting Information. The conductive-bridge-neuron device, having a simple vertical device structure with a 100-nm-thick CuTe top electrode, 15-nm-thick $TiO_2$ resistive layer, and 100-nm-thick TiN bottom electrode, could successfully implement the integrate function by controlling the Cu filaments in the $TiO_2$ resistive layer. Specifically, a larger

number of input-current spikes led to thinner Cu filaments. Moreover, a spiking conductive-bridge-neuron was designed using a current-mirror-type sense amplifier, latch, MCU, and DACs. The framework could exhibit an integrate-and-fire function, depending on the input-voltage-spike amplitude supplied from the DAC: a higher input-voltage spike led to a higher generation frequency of fire spikes. In addition, an SNN was effectively designed with a conductive-bridge neuron as the hardware part and input spike generation module, weight update strategy based on the simplified STDP algorithm, and GUI as the software part. The designed SNN could realize real-time correlation detection with online learning. In particular, with the increase in the number of learning iterations, the normalized weight for the synapses connected with the correlated and uncorrelated input neurons increased gradually and decreased steadily, respectively. Furthermore, a synapse array could be realized by using a cross-point-conductive-bridge-memristor array, as shown in Figure S10a, Supporting Information. Cross-point conductive-bridge-memristor synapse devices could be produced using the same device structure as that of the conductive-bridge-neuron because the conductive-bridge-memristor synapse presented potentiation and depression behavior, as shown in Figure S10d, Supporting Information. Such an array, as shown in Figure S10a, Supporting Information, has several advantages and can help ensure a simple fabrication process and low production cost for neuromorphic chips because the synapses and neurons can be simultaneously fabricated with the same device structure. Notably, in the case of C-MOSFET-based neuromorphic chips, a synapse is generally produced by eight n- and p-MOSFETs, and a neuron is fabricated using capacitors and C-MOSFETs. The proposed framework can help realize a cross-point-memristor array connected with an input neuron and output conductive-bridge-neuron to achieve a high neuronal density. However, since most of power in the conductive-bridge-neuron would be dissipated by the conductive-bridge-neuron device, for achieving low power consumption, further study is necessary for reducing the integrate current in the conductive-bridge-neuron device; that is, from 100 (our work) to less than 1 μA. In addition, further study is necessary for improving symmetricity, although this conductive-bridge-synapse device has an excellent linearity of potentiation, as shown in Figure S10d, Supporting Information.

## 4. Experimental Section

*Conductive-Bridge-Neuron Device Fabrication*: A 100-nm-thick $SiO_2$ film was grown on a silicon substrate. A 100-nm-thick TiN bottom electrode having a width of 5 μm was patterned using the first lift-off process. This process was followed by the spin coating of a positive photoresist (AZ5214E) at 5000 rpm for 30 s, soft baking at 120 °C for 1 min 40 s, exposure to UV light with a beam intensity of 20 mW $cm^{-2}$ for 12 s, development of the exposed patterned photoresist by using a developer (AZ300MIF) for 70 s, DC magnetron sputtering at a TiN power of 40 W and 30 sccm Ar flow, and lift-off of the patterned photoresist, as shown in Figure 1a. Next, a 15-nm-thick $TiO_2$-film resistive layer and 100-nm-thick CuTe top electrode having a width of 5 μm were patterned via the second lift-off process that was similar to the first lift-off process. The difference was that the 15-nm-thick $TiO_2$-film resistive layer was sputtered at 40 W RF power under a 40 sccm Ar flow, and the 100-nm-thick CuTe top electrode was sputtered at a 40 W DC power under a 30 sccm Ar flow. The area of the conductive-bridge neuron device was 25 $\mu m^2$, as shown in Video S1, Supporting Information. To characterize the shape of Cu filaments in the $TiO_2$ resistive layer, a cross-sectional transmission-electron-microscope image of the conductive-bridge-neuron device was observed at an acceleration voltage of 200 KeV, and the depth profile of the Cu ion concentration of the conductive-bridge-neuron device was measured through energy-dispersive X-ray spectroscopy (TEM and EDS: JEM-2100F). In addition, the crystallinity of the $TiO_2$ resistive layer was characterized by X-ray diffraction (ATX-G). Moreover, ToF-SIMS (TOF.SIMS 5) measurement was performed to investigate precise Cu ion concentration depending on the number of input-current-spikes. The electrical properties and integrate function of the conductive-bridge-neuron device were evaluated using a source measurement unit (Keithley 236) and semiconductor parameter analyzer (Agilent B2902A).

*Formation or Rupturing of Cu Filaments in Conductive-Bridge-Neuron Device*: The changes in the resistance of the conductive-bridge-neuron device from the HRS (i.e., the detachment of Cu filaments on the TiN bottom electrode) to the LRS (i.e., the attachment of the conductive Cu filaments on the TiN bottom electrode) could be explained by the formation of the conductive Cu filaments in the $TiO_2$ resistive layer. The CuTe top electrode supplied $Cu^{2+}$ ions to the $TiO_2$ resistive layer via oxidation. The oxidation probability and migration probability of $Cu^{2+}$ ions are presented in Supporting Information Note.

*Input Spike Generation for Correlation Detection*: To generate the correlated and uncorrelated pre-spike signals, 1000 Gaussian random values were generated from a multivariate-normal-probability-density function:

$$f_{x_1,\ldots,x_N}(x_1,\ldots,x_N)=\frac{\left|[C_X]^{-1}\right|^{1/2}}{(2\pi)^{N/2}}\exp\left\{-\frac{\left[x-\overline{X}\right]^{T}[C_X]^{-1}\left[x-\overline{X}\right]}{2}\right\} \quad (1)$$

$$[C_X]=\begin{bmatrix} C_{11} & \cdots & C_{1N} \\ \vdots & \ddots & \vdots \\ C_{N1} & \cdots & C_{NN} \end{bmatrix} \quad (2)$$

$[C_X]$, $C_{ij}$, and $\overline{X}$ denoted the covariance matrix in Equation (2), covariance (between $i$ and $j$ entries), and mean spike generation probability, respectively. The Gaussian random number $X$ at a specific $C_X$ was generated, as defined in Equation (3), and transformed to a uniform distribution $U$ by using a normal cumulative density function, specified by Equation (4)

$$X \approx f\left(\overline{X},C_X\right) \quad (3)$$

$$U=\Psi(X) \quad (4)$$

Here, $f(\overline{X},C_X)$ and $\Psi(X)$ denoted the multivariate-normal-probability-density function in Equation (1) and normal cumulative density function, respectively. $U$ could be transformed to any probability density function by using a proper probability density function. In the authors' case, the uniform distribution was transformed to a Poisson distribution with parameter $\lambda$, which described the average number of events. Figure 5a shows the time evolution of the generated pre-spike signals (100 correlated + 900 uncorrelated spike signals). Because 100 pre-spike signals were correlated with a covariance of 0.5, 100 pre-spike signals fired at a similar time, as shown in Figure 5b. In contrast, the 900 uncorrelated pre-spike signals occurred independent of one another, as shown in Figure 5c.

*System Setup for Correlation Detection*: The hardware and software mixed SNN was designed to perform correlation detection using conductive-bridge neuron. All components such as neuron devices, drive circuits, and control systems related to conductive-bridge neuron were implemented in hardware. Then, the parts related to pre-neurons and synapses (including updating of synaptic weights) were implemented in software. The circuit was precisely controlled by a MCU (ATmega2560).

For the operation of the MCU, the code written in C language was uploaded to the MCU. The MCU sent and received signals to and from the computer via serial communication. On the software part, a custom GUI written in Python was used to communicate with the MCU. Each part of the hardware such as circuit drive voltage, circuit signal timing, and output spike monitoring could be controlled via GUI. A drive circuit consisted of a current-mirror-type sense amplifier, latch, several MOSFETs (n-MOSFET; 2N7000, p-MOSFET; BS250), bypass capacitor (0.1 μF), and resistors (1 kΩ, 10 kΩ). The DC level of each control signal was precisely adjusted using a 16-bit DAC (LTC1655) controlled by the MCU. At each read cycle, the MCU read the output spike signal and confirmed that the conductive-bridge neuron produced an output spike. When an output spike signal was detected, the MCU notified the computer that a spike had occurred. At this time, the software updated the software synapse by calculating the time difference between the software-generated input spikes and the hardware neurons-generated output spikes. Simplified STDP algorithm was used to update the weights.

## Supporting Information

Supporting Information is available from the Wiley Online Library or from the author.

## Acknowledgements

D.-W.K. and D.-S.W. contributed equally to this work. This research was supported by National R&D Program through the National Research Foundation of Korea (NRF) funded by Ministry of Science and ICT(2021M3F3A2A01037733), the MOTIE (Ministry of Trade, Industry & Energy [10068055]), and KSRC (Korea Semiconductor Research Consortium) support program for the development of the future semiconductor device, and BrainKorea21 Four.

## Conflict of Interest

The authors declare no conflict of interest.

## Data Availability Statement

The data that support the findings of this study are available from the corresponding author upon reasonable request.

## Keywords

artificial intelligence, conductive-bridge neurons, correlation detection, neuromorphic computing, online learning, spiking neural networks

Received: December 14, 2021
Revised: January 17, 2022
Published online: February 25, 2022

[1] M. Kleppmann, *Designing Data-Intensive Applications*, 1st ed., O'Reilly Media, Inc., Sebastopol, California **2017**.
[2] C. L. P. Chen, C. Y. Zhang, *Inf. Sci.* **2014**, *275*, 314.
[3] S. Ghose, A. Boroumand, J. S. Kim, O. Mutlu, *IBM J Res Dev.* **2019**, *63*, 6.
[4] J. R. Hollerman, W. Schultz, *Nat. Neurosci.* **1998**, *1*, 304.
[5] A. A. Grace, B. S. Bunney, *J. Neurosci.* **1984**, *4*, 2877.
[6] K. Roy, A. Jaiswal, P. Panda, *Nature* **2019**, *575*, 607.
[7] A. Sebastian, M. L. Gallo, R. Khaddam-Aljameh, E. Eleftheriou, *Nat. Nanotechnol.* **2020**, *15*, 529.
[8] W. Zhang, B. Gao, J. Tang, P. Yao, S. Yu, M. F. Chang, H. J. Yoo, H. Qian, H. Wu, *Nat. Electron.* **2020**, *3*, 371.
[9] P. A. Merolla, J. V. Arthur, R. Alvarez-icaza, A. S. Cassidy, J. Sawada, F. Akopyan, B. L. Jackson, N. Imam, C. Guo, Y. Nakamura, B. Brezzo, I. Vo, S. K. Esser, R. Appuswamy, B. Taba, A. Amir, M. D. Flickner, W. P. Risk, R. Manohar, D. S. Modha, *Science* **2014**, *345*, 668.
[10] L. J. Gentet, G. J. Stuart, J. D. Clements, *Biophys. J.* **2000**, *79*, 314.
[11] G. Indiveri, B. Linares-Barranco, R. Legenstein, G. Deligeorgis, T. Prodromakis, *Nanotechnology* **2013**, *24*, 384010.
[12] A. Basu, P. E. Hasler, *IEEE Trans. Circuits Syst. I: Regul. Pap.* **2010**, *57*, 2938.
[13] G. Indiveri, E. Chicca, R. Douglas, *IEEE Trans. Neural Networks* **2006**, *17*, 211.
[14] S. A. Aamir, P. Müller, A. Hartel, J. Schemmel, K. Meier, *ESSCIRC Conf. 2016: 42nd European Solid-State Circuits Conf.*, IEEE, Piscataway, NJ **2016**, pp. 71–74, https://doi.org/10.1109/ESSCIRC.2016.7598245.
[15] A. Joubert, B. Belhadj, O. Temam, R. Héliot, *The 2012 Int. Joint Conf. on Neural Networks (IJCNN)*, IEEE, Piscataway, NJ **2012**.
[16] I. Sourikopoulos, S. Hedayat, C. Loyez, F. Danneville, V. Hoel, E. Mercier, A. Cappy, *Front. Neurosci.* **2017**, *11*, 123.
[17] J. H. B. Wijekoon, P. Dudek, *Neural Networks* **2008**, *21*, 524.
[18] X. Wu, V. Saxena, K. Zhu, S. Balagopal, *IEEE Trans. Circuits Syst. II: Express Briefs* **2015**, *62*, 1088.
[19] T. Tuma, A. Pantazi, M. L. Gallo, A. Sebastian, E. Eleftheriou, *Nat. Nanotechnol.* **2016**, *11*, 693.
[20] R. A. Cobley, H. Hayat, C. D. Wright, *Nanotechnology* **2018**, *29*, 195202.
[21] J. Lin, J. S. Yuan, *2017 IEEE Biomedical Circuits and Systems Conf. (BioCAS)*, IEEE, Piscataway, NJ **2018**, pp. 1–4, https://doi.org/10.1109/BIOCAS.2017.8325169.
[22] S. Lashkare, S. Chouhan, T. Chavan, A. Bhat, P. Kumbhare, U. Ganguly, *IEEE Electron Device Lett.* **2018**, *39*, 484.
[23] H. Aziza, M. Moreau, A. Perez, A. Virazel, P. Girard, *2019 17th IEEE Int. New Circuits and Systems Conf. (NEWCAS)*, IEEE, Piscataway, NJ **2019**, pp. 1–4, https://doi.org/10.1109/NEWCAS44328.2019.8961278.
[24] J. Woo, D. Lee, Y. Koo, H. Hwang, *Microelectron. Eng.* **2017**, *182*, 42.
[25] X. Wang, P. Huang, Z. Dong, Z. Zhou, Y. Jiang, R. Han, L. Liu, X. Liu, J. Kang, *2018 Int. Symp. on VLSI Technology, Systems and Application (VLSI-TSA)*, IEEE, Piscataway, NJ **2018**, pp. 1–2, https://doi.org/10.1109/VLSI-TSA.2018.8403854.
[26] M. W. Kwon, S. Kim, M. H. Kim, J. Park, H. Kim, S. Hwang, B. G. Park, *J. Nanosci. Nanotechnol.* **2017**, *17*, 3038.
[27] K. Wang, Q. Hu, B. Gao, Q. Lin, F. W. Zhuge, D. Y. Zhang, L. Wang, Y. H. He, R. H. Scheicher, H. Tong, X. S. Miao, *Mater. Horiz.* **2021**, *8*, 619.
[28] S. Dutta, V. Kumar, A. Shukla, N. R. Mohapatra, U. Ganguly, *Sci. Rep.* **2017**, *7*, 8257.
[29] K. H. Kwon, D. W. Kim, H. J. Kim, S. M. Jin, D. S. Woo, S. H. Park, J. G. Park, *J. Mater. Chem. C* **2020**, *8*, 8125.
[30] K. C. Kwon, M. J. Song, K. H. Kwon, H. V. Jeoung, D. W. Kim, G. S. Lee, J. P. Hong, J. G. Park, *J. Mater. Chem. C* **2015**, *3*, 9540.
[31] M. J. Song, K. H. Kwon, J. G. Park, *Sci. Rep.* **2017**, *7*, 3065.
[32] T. Hitosugi, N. Yamada, S. Nakao, Y. Hirose, T. Hasegawa, *Phys. Status Solidi A* **2010**, *207*, 1529.
[33] M. Li, F. Zhuge, X. Zhu, K. Yin, J. Wang, Y. Liu, C. He, B. Chen, R. W. Li, *Nanotechnology* **2010**, *21*, 425202.
[34] K. J. Gan, P. T. Liu, T. C. Chien, D. B. Ruan, S. M. Sze, *Sci. Rep.* **2019**, *9*, 14141.

[35] N. Xu, B. Gao, L. F. Liu, B. Sun, X. Y. Liu, R. Q. Han, J. F. Kang, B. Yu, *2008 Symp. on VLSI Technology*, IEEE, Piscataway, NJ **2008**, pp. 100–101, https://doi.org/10.1109/VLSIT.2008.4588578.
[36] X. Ding, Y. Feng, P. Huang, L. Liu, J. Kang, *Nanoscale Res. Lett.* **2019**, *14*, 157.
[37] X. Zhang, L. Xu, H. Zhang, J. Liu, D. Tan, L. Chen, Z. Ma, W. Li, *Nanoscale Res. Lett.* **2020**, *15*, 11.
[38] S. Lee, J. Song, S. Lim, S. A. Chekol, H. Hwang, *Solid-State Electron.* **2019**, *153*, 8.
[39] L. Goux, K. Opsomer, R. Degraeve, R. Mller, C. Detavernier, D. J. Wouters, M. Jurczak, L. Altimime, J. A. Kittl, *Appl. Phys. Lett.* **2011**, *99*, 053502.
[40] A. L. Hodgkin, A. F. Huxley, *Bull. Math. Biol.* **1990**, *52*, 500.
[41] E. M. Izhikevich, *IEEE Trans. Neural Networks* **2003**, *14*, 1569.
[42] D. W. Kim, W. S. Yi, J. Y. Choi, K. Ashiba, J. U. Baek, H. S. Jun, J. J. Kim, J. G. Park, *Front. Neurosci.* **2020**, *14*, 309.
[43] C. V. Parise, M. O. Ernst, *Nat. Commun.* **2016**, *7*, 11543.
[44] C. V. Parise, C. Spence, M. O. Ernst, *Curr. Biol.* **2012**, *22*, 46.
[45] C. Spence, *Ann. N. Y. Acad. Sci.* **2013**, *1296*, 31.
[46] P. Z. Peebles, *Probability Random Variables and Random Signal Prinsiples*, 1st ed., McGraw-Hill Education, Americas, NY **2015**.
[47] J. M. Cruz-Albrecht, M. W. Yung, N. Srinivasa, *IEEE Trans. Biomed. Circuits Syst.* **2012**, *6*, 246.